This article has been accepted for publication in a future issue of this journal, but has not been fully edited. Content may change prior to final publication. Citation information: DOI 10.1109/TNSRE.2021.3107142, IEEE Transactions on Neural Systems and Rehabilitation Engineering

BECT Spike Detection based on Novel EEG Sequence Features and LSTM Algorithms

Zhendi Xu*, Tianlei Wang, Jiuwen Cao†, *Senior Member, IEEE,* Zihang Bao, Tiejia Jiang*, and Feng Gao†

***Abstract*—The benign epilepsy with spinous waves in the central temporal region (BECT) is the one of the most common epileptic syndromes in children, that seriously threaten the nervous system development of children. The most obvious feature of BECT is the existence of a large number of electroencephalogram (EEG) spikes in the Rolandic area during the interictal period, that is an important basis to assist neurologists in BECT diagnosis. With this regard, the paper proposes a novel BECT spike detection algorithm based on time domain EEG sequence features and the long short-term memory (LSTM) neural network. Three time domain sequence features, that can obviously characterize the spikes of BECT, are extracted for EEG representation. The synthetic minority oversampling technique (SMOTE) is applied to address the spike imbalance issue in EEGs, and the bi-directional LSTM (BiLSTM) is trained for spike detection. The algorithm is evaluated using the EEG data of 15 BECT patients recorded from the Children's Hospital, Zhejiang University School of Medicine (CHZU). The experiment shows that the proposed algorithm can obtained an average of 88.54% F1 score, 92.04% sensitivity, and 85.75% precision, that generally outperforms several state-of-the-art spike detection methods.**

***Index Terms*—BECT, Spike detection, Time domain EEG sequence features, LSTM model**

I. Introduction

As a common neurological disease, the incidence of epilepsy in children is 10∼15 times as high as that of adults. Benign childhood epilepsy with centro-temporal spikes (BECT), also known as the childhood benign rolandic epilepsy, is the most common focal epilepsy in childhood, accounting for 15%∼24% of all childhood epilepsy [1, 2]. BECT has a low probability of having seizures. Therefore, the electroencephalograms (EEGs) recorded from the interictal period become the main data to help doctors analyze the condition of BECT patients.

Z. Xu, T. Wang, J. Cao, and Z. Bao are with Machine Learning and I-health International Cooperation Base of Zhejiang Province, and Artificial Intelligence Institute, Hangzhou Dianzi University, Zhejiang, China, 310018. J. Cao is also with Research Center for Intelligent Sensing, Zhejiang Lab, Hangzhou 311100, China.

T. Jiang and F. Gao are with the Department of Neurology, The Children's Hospital, Zhejiang University School of Medicine, National Clinical Research Center for Child Health, Hangzhou 310003, China.

†J. Cao and F. Gao are the corresponding authors, *Contribute equally to the paper.

E-mail: 954401521@qq.com, tianlei.wang.cn@gmail.com, jwcao@hdu.edu.cn, 863273751@qq.com, jiangyouze@zju.edu.cn, epilepsy@zju.edu.cn.

This work was supported by the National Natural Science Foundation of China (U1909209), the National Key Research and Development Program of China (2021YFE0100100, 2021YFE0205400), the Open Research Projects of Zhejiang Lab (2021MC0AB04), the Key Research and Development Program of Zhejiang Province (2020C03038), and Zhejiang Provincial Natural Science Foundation (LBY21H090002).

To assist clinical analysis, EEG features appearing in epilepsy are summarized as biomarkers by neurobiologists. Epileptiform discharge is a typical biomarker, generally including spike, sharp, spike and wave complex, and sharp and wave complex [3]. With the upgrade of EEG acquisition equipment, more and more high-frequency EEG signals, such as ripples and fast ripples, have been used as epilepsy biomarkers, leading to good results [4]. The diagnosis of BECT is one of the typical cases in epileptiform discharge analysis. The most obvious feature of the interical EEG of BECT patients is the large number of spike and sharp wave complexes in the Rolandic area. On the EEG International 10-20 system [5], the midtemporal and central areas have the highest discharge amplitude [6]. The width of the spikes and sharps is generally around 50-100 ms, the amplitude is mostly greater than 100 μV, and are usually prominent in the background activity. Since the generation mechanism and physiological significance of spike and sharp are basically similar, there is generally no obvious difference in waveforms except for the duration. Therefore, in this paper, we uniformly use the spike to refer to spike and sharp waves.

Traditionally, to have a better diagnosis of BECT patients, neurologists have to analyze the EEG data to find the epileptiform discharges in the millisecond level, which is extremely tedious and time-consuming. With this regard, we develop a novel BECT spike detection algorithm based on the time domain EEG sequence features and the enhanced long short-term memory (LSTM) neural network model. The contributions of the paper are three-fold: 1) two time domain EEG sequence features, the smooth nonlinear energy (SNE) and morphological characteristics, are extracted to characterize spikes, 2) to address the imbalance issue existed between spike and non-spike signals, the synthetic minority oversampling technique (SMOTE) is applied to generate synthetic spike sample for model learning, 3) a stacked bi-directional LSTM (BiLSTM) model is designed to enhance the spike detection accuracy. The effectiveness of the proposed spike detection algorithm is validated by using the EEG data of 15 BECT patients recorded from the Children's Hospital, Zhejiang University School of Medicine (CHZU). Experimental comparisons to 5 state-of-the-art (SOTA) spike detection methods are also presented in the paper to demonstrate the superiority of the proposed algorithm. Fig. 1 explicitly shows the flow chart of the developed spike detection algorithm in the paper.

II. Related works

As a common epilepsy biomarker, spike has broad applications in the auxiliary diagnosis [7, 8] and seizure prediction

This article has been accepted for publication in a future issue of this journal, but has not been fully edited. Content may change prior to final publication. Citation information: DOI 10.1109/TNSRE.2021.3107142, IEEE Transactions on Neural Systems and Rehabilitation Engineering

[9]. The earliest study can be traced back to 1972, in which Steven et al. [10] tried to explore the correlation between spikes and seizures using the power spectrum of EEGs. Gotman et al. [11] decomposed EEG into half-waves and extracted its features for the spike detection. Qian et al. [12] used the cascade of the difference filter and the product operator to enhance the spike amplitude. Liu et al. [13] eliminated background noise in EEGs with a morphological filter which adopts adaptive Gaussian structure factor. Oikonomou et al. [14] established a time-varying autoregressive model based on the non-stationarity of EEGs, and used a Kalman filter to estimate the time-varying coefficients, which enhanced the signal-to-noise ratio. More fundamental spike detection methods can be referred to [15–19]. In general, most spike detection algorithms tend to use time domain features. Although the frequency domain and wavelet domain features are widely used in the field of EEG signal processing [20, 21], their application in spike detection [22–25] is limited due to the short duration of the target waveform and high positioning accuracy requirements.

Recently, machine learning based neural networks have been widely used for EEG analysis, such as epilepsy and seizure detection [26–29], spike detection [30–32], brain-computer interfaces [33–35], etc. Webber et al. [30] implemented spike detection algorithms through spike candidate selection and artificial neural networks (ANN) based classification. Özdamar et al. [31] directly adopted ANN to learn on the raw EEGs, and explored the influence of the feature input dimension and network structure parameters. Medvedev et al. [32] used the relative spectral power of different frequency bands as the features, and employed BiLSTM for spikes, ripples, and composite waveforms detection. Johansen et al. [36] applied one-dimensional convolutional neural network (CNN) to spike detection. Many other representative deep learning based spike detections can be referred to [37, 38]. Particularly, for childhood BECT spike detection, Wang et al. [39] developed a hybrid algorithm based on an adaptive template matching algorithm and a random forest (RF) classifier for false positives elimination. Besides [39], few attentions have been paid to the BECT spike detection.

III. Methodology

A. EEG Preprocessing

Interferences, such as eye blinking, electromyogram (EMG), non-physiological artifacts, baseline drift, etc. (shown in Fig. 2), usually affect the performance in scalp EEG analysis [40, 41]. Preliminary frequency domain filtering by a 50 Hz IIR notch filter and a 1∼70 Hz IIR filter is applied to remove the power frequency noise, to reduce low-frequency interference such as baseline drift, and to suppress the high-frequency interference. Then, the following preprocessing is adopted.

1) Savitzky-Golay Filtering: The Savitzky-Golay filter (S-G filter) is a time domain polynomial least squares filtering algorithm, which is effective to eliminate noise while remain the signal distribution characteristics unchanged. Part of the interference caused by electromyography and poor contact also has high-frequency spike-like characteristics, but its amplitude and duration are generally smaller than spikes. By applying the S-G filter, these interferences can be smoothed under the premise of not having a great impact on spikes, and the influence on subsequent spike identification can be reduced.

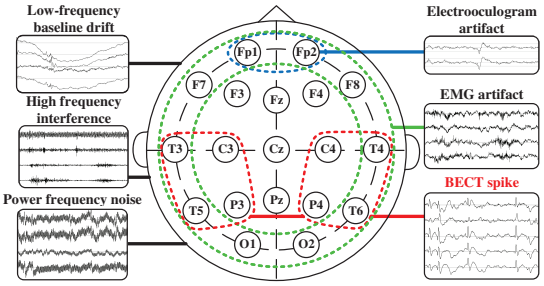

Fig. 2. The 10-20 international standard EEG recording system, the waveform and appearance position of EEG interferences and spikes.

Suppose the width of the filter window is $n = 2m + 1$, the original EEG is x, and the k-order S-G filter will fit the data using a k degree polynomial defined as $y = a_0 + a_1 x + a_2 x^2 + \cdots + a_k x^k$, where a_i $(i = 0, \ldots, k)$ is the polynomial coefficient. For all EEG segments, the following k-ary linear equation can be obtained

$$\begin{bmatrix} y_{-m} \\ \vdots \\ y_m \end{bmatrix} = \begin{bmatrix} x(1) & \cdots & x^k(-m) \\ \vdots & \vdots & \vdots \\ x(1) & \cdots & x^k(m) \end{bmatrix} \begin{bmatrix} a_0 \\ \vdots \\ a_k \end{bmatrix} + \begin{bmatrix} e_{-m} \\ \vdots \\ e_m \end{bmatrix}$$

where e is the fitting error. The matrix form is

$$\boldsymbol{Y}_{(2m+1)\times 1} = \boldsymbol{X}_{(2m+1)\times k}\boldsymbol{a}_{k\times 1} + \boldsymbol{e}_{(2m+1)\times 1} \quad (1)$$

where $\boldsymbol{Y}_{(2m+1)\times 1}$, $\boldsymbol{X}_{(2m+1)\times k}$, $\boldsymbol{a}_{k\times 1}$, $\boldsymbol{e}_{(2m+1)\times 1}$ are the matrix/vector forms of variables in (1). By least squares, $\hat{\boldsymbol{a}}$ can be estimated as $\hat{\boldsymbol{a}} = (\boldsymbol{X}^T\boldsymbol{X})^{-1}\boldsymbol{X}^T\boldsymbol{Y}$, and the filtered output is

$$\hat{\boldsymbol{Y}} = \boldsymbol{X}\hat{\boldsymbol{a}} = \boldsymbol{X}(\boldsymbol{X}^T\boldsymbol{X})^{-1}\boldsymbol{X}^T\boldsymbol{Y}. \quad (2)$$

The center sequence $\hat{\boldsymbol{Y}}(0)$ of the filtered output is finally used.

In this paper, the filter window length is set to 71, and the corresponding duration is 0.071 s, which is close to the average duration of BECT spikes. It can ensure that the interval contains enough information to minimize the impact on spikes, and meanwhile ensure that the noises with a duration shorter than spikes. Through experiments, the third-order filter has the best overall performance and good smoothing effect on noises. Fig. 3 shows the filtered EEGs obtained by frequency-domain filter and S-G filter, respectively.

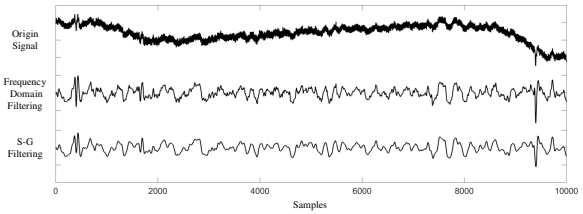

Fig. 3. EEG preprocessing by the frequency domain filter and the S-G filter.

This article has been accepted for publication in a future issue of this journal, but has not been fully edited. Content may change prior to final publication. Citation information: DOI 10.1109/TNSRE.2021.3107142, IEEE Transactions on Neural Systems and Rehabilitation Engineering

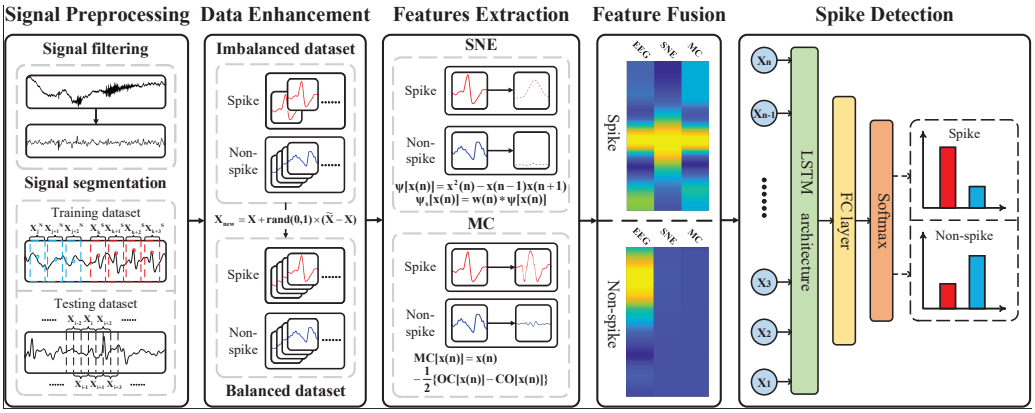

Fig. 1. The flowchart of the proposed BECT spike detection algorithm.

2) Standardization: EEG normalization can help to reduce the sensitivity of different acquisition devices. Commonly used resizing methods include rescaling, mean normalization and Z-score normalization. Since the scalp EEG is sensitive to external interferences, using rescaling or mean normalization may not have a satisfactory normalization. Since the preprocessing is performed on the entire signal, the Z-score normalization is the most suitable method here, defined as

$$x' = \frac{x - \text{mean}(x)}{\sigma} \tag{3}$$

where x is the EEG signal, mean(x) and σ are the mean and variance, that can be estimated from the samples.

3) Data Segmentation: The EEG frame length is set to be 0.2 s by considering the duration of BECT spikes. For model training and validation, the pre-marked points are directly divided to obtain samples, while in testing, we set a 50% overlap rate to continuously divide the entire EEGs into frames. The purpose is to visually analyze the detection performance on real data, and also to ensure the integrity of the spike waveform in the sample interval.

B. Data Augmentation

Compared with the long-term EEG recordings, the duration of the EEG in the non-spike state is usually much longer than spikes. Fig. 4 shows the spike duration ratios recorded from 15 BECT patients in the CHZU database. As observed, for most patients, the proportion of spike discharge durations with respect to the whole recordings is less than 6%, and the proportion of spike of 5 patients is even less than 2%. This leads to a typical imbalance data learning problem. It is also well known that conventional machine learning models are generally not applicable to imbalance data, and usually suffer poor performance on the minority classes, resulting in a very low recall rate. Therefore, we recur to the SMOTE [42] resampling method to generate minority samples (spikes), where the generated spikes will be only used in model training.

SMOTE is an improved random oversampling algorithm, that can effectively address the overfitting and poor generalization issues in the basic random oversampling methods. SMOTE overcomes these issues by exploring the nearest

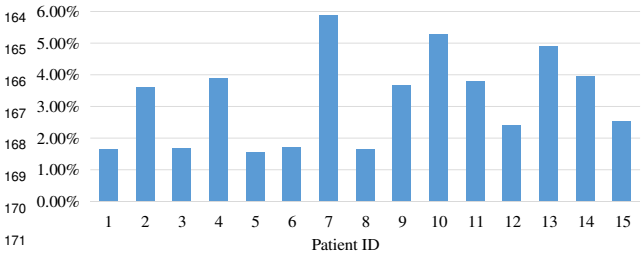

Fig. 4. Spike discharge duration proportion in each patient's EEG in the CHZU database (the duration of one spike discharge is around 0.075 s).

neighbors within the minority category to generate the synthetic samples x_{new} using $x_{new} = x + \text{rand}(0,1) \times (\widetilde{x} - x)$, where x is the sample from the minority class, $\widetilde{x}$ is randomly selected from the K nearest neighbors of x.

C. Time domain Sequence Feature Extraction

Two time domain features, smooth nonlinear energy (SNE) and morphological characteristics (MC), which can reflect the characteristics of EEGs and distinguish spikes from non-spikes are extracted for signal representation in this paper. The dimensions of SNE and MC are consistent with that of EEG segment to ensure that they can be applied for the subsequent model learning.

1) Smooth nonlinear energy: The nonlinear energy operator (NEO) was proposed by Kaiser for nonlinear speech modeling [43]. NEO can characterize the instantaneous frequency and amplitude of the signal, and its output is proportional to the product of the amplitude and frequency of the input.

Let $x(t)$ $(t > 0)$ be a continuous time signal, NEO is

$$\psi[x(t)] = x^2(t) - x(t)x''(t) \tag{4}$$

where $\psi[x(t)]$ is the nonlinear energy (NE) and $x''(t)$ is the second-order derivative. For a discrete signal $x(n)$, NEO is

$$\psi[x(n)] = x^2(n) - x(n-1)x(n+1). \tag{5}$$

To further improve the ability of NEO in characterizing non-stationary signals, a smooth nonlinear energy operator (SNEO) has been developed in [44] as

$$\psi_s[x(n)] = w(n) * \psi[x(n)] \tag{6}$$

This article has been accepted for publication in a future issue of this journal, but has not been fully edited. Content may change prior to final publication. Citation information: DOI 10.1109/TNSRE.2021.3107142, IEEE Transactions on Neural Systems and Rehabilitation Engineering

where $w(n)$ is the triangular window function, $*$ represents the convolution operation, and $\psi_s[x(n)]$ is the SNE.

SNE reduces the interference through the convolution operation. As shown in Fig. 5, SNE from the spike discharge interval is much higher than that from the background and non-spike EEG. Therefore, the spike can be clearly protruded from a segment of EEGs by SNE.

2) Morphological characteristics: Morphological filter is a nonlinear filter based on the basic mathematical morphological transformation. It was originally used to process binary images. Later, Serra et al. [45] introduced the set representation method of functions and extended it to time sequence signal processing. For the signal $x(n)$, $n \in (0, 1, \cdots, N-1)$ and the structure element $g(m)$, the four basic morphological operations of $g(m)$ with respect to $x(n)$ are corrosion '$\ominus$', expansion '$\oplus$', morphological opening '$\circ$', and morphological closing '$\bullet$', which are respectively defined as

$$(x \ominus g)(n) = min[x(n+m) - g(m)] \quad (7)$$

$$(x \oplus g)(n) = max[x(n+m) - g(m)] \quad (8)$$

$$(x \circ g)(n) = (x \ominus g) \oplus g \quad (9)$$

$$(x \bullet g)(n) = (x \oplus g) \ominus g \quad (10)$$

where $m = 0, \ldots, M-1$ and $N \geq M$. Corrosion operation removes the negative phase peak and reduces the width of the positive phase peak, expansion operation removes the positive phase peak and reduces the width of the negative phase peak, the open operation only removes the positive phase peak, and the closed operation only removes the negative phase peak.

To further improve the filtering performance, the basic operations mentioned above are cascaded and combined to better separate the target from the original signal. The morphological opening-closing operation (OC), closing-opening operation (CO) and open-close-closed-open average combined operation (OCCO) are respectively defined as

$$OC[x(n)] = [(x \circ g) \bullet g](n) \quad (11)$$

$$CO[x(n)] = [(x \bullet g) \circ g](n) \quad (12)$$

$$OCCO[x(n)] = \frac{1}{2}\{OC[x(n)] + CO[x(n)]\}. \quad (13)$$

OC and CO can effectively separate positive and negative pulses from the signal, respectively. Due to the inverse scalability of the open and closed operations, a single OC or OC operation will cause statistical deviation. OCCO eliminates statistical deviations and improves the filtering performance by averaging OC and CO results.

After the structure element setting, OCCO can filter out the spike wave-like waveform. Subtracting the result of OCCO from the original EEG, the characteristic sequence containing only the waveform of the type structure unit is

$$MC(n) = x(n) - OCCO[x(n)]. \quad (14)$$

The structural element used here is a positive half-wave Sine signal with a certain degree of similarity to the spike wave, defined as

$$g(m) = h_s \sin\left(\frac{\pi m}{t_s}\right) \quad (15)$$

where h_s is the spike amplitude, t_s is the spike duration, and $m \in (0, 0.001, \cdots, t_s)$.

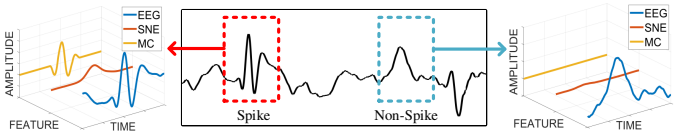

Fig. 5. Original EEG, smooth nonlinear energy and morphological characteristics of spike and non-spike samples.

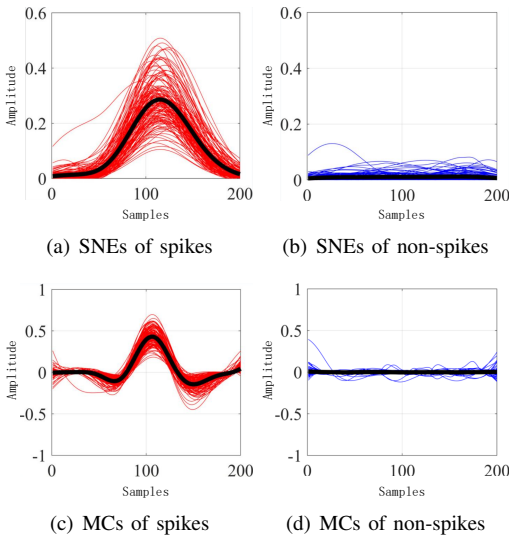

(a) SNEs of spikes (b) SNEs of non-spikes

(c) MCs of spikes (d) MCs of non-spikes

Fig. 6. Comparisons on SNEs and MCs obtained on multiple spikes and non-spikes from the EEGs of a BECT patient.

Fig. 5 plots the typical BECT spike and non-spike EEG samples, and their corresponding SNE and MC features. As observed, for both the SNE and MC features, the waveform of spike is well retained, and the amplitudes of the two features obtained from non-spike EEGs are apparently suppressed. For further validation, we have compared the SNE and MC features obtained from 139 spikes and 1455 non-spikes from a BECT patient of the CHZU database in Fig. 6. For non-spike EEGs, the SNE and MC features are generally around 0, while on the contrary, spike EEGs show completely different SNE and MC features to non-spikes.

D. LSTM Architecture Neural Network Classifier

Instead of directly adopting the SNE and MC features for spike detection, we apply the LSTM neural network with the stacked bi-directional structure for discriminative feature learning and spike EEG detection. Conventional RNN generally uses simple repeating module containing only one tanh layer for time series learning. LSTM modifies the repeating module, designs the cell state that stores important information and controls it through three gate structures, namely the forget gate, input gate and output gate [46]. It can overcome the gradient disappearance and explosion issues existed in traditional RNN. The forget gate selectively forgets the information passed from the previous unit, defined as

$$f_t = \sigma(W_f \cdot [h_{t-1}, x_t] + b_f) \quad (16)$$

This article has been accepted for publication in a future issue of this journal, but has not been fully edited. Content may change prior to final publication. Citation information: DOI 10.1109/TNSRE.2021.3107142, IEEE Transactions on Neural Systems and Rehabilitation Engineering

where x is the input sequence, h_{t-1} is the output of the previous block, c_{t-1} is the cell state of the previous memory unit, b_f and w_f are the bias and weight vectors, σ is the sigmoid activation function, and f_t is the output, determining how much of the cell state from the previous moment is retained to the current moment unit state c_t.

The input gate of LSTM selectively records new information into the cell state, with the definition as

$$i_t = \sigma(W_t \cdot [h_{t-1}, x_t] + b_i) \tag{17}$$

$$\widetilde{C}_t = tanh(W_C \cdot [h_{t-1}, x_t] + b_C) \tag{18}$$

where i_t determines how much input is retained in the current moment unit state C_t, and $\widetilde{C}_t$ is the current input unit state. The cell state is then updated by

$$C_t = f_t * C_{t-1} + i_t * \widetilde{C}_t. \tag{19}$$

Finally, the input gate will obtain the output of the current block based on the cell state as

$$o_t = \sigma(W_o[h_{t-1}, x_t] + b_o) \tag{20}$$

$$h_t = o_t * tanh(C_t). \tag{21}$$

Bidirectional LSTM (BiLSTM) and stacked LSTM are two variants of LSTM. BiLSTM contains forward and backward structures in a unit. Stacked LSTM uses a cascade method to obtain a deeper structure. At the same time, these two structures can also be superimposed to get a more complex architecture.

In this paper, we have developed 4 types of LSTM based BECT spike detection models, including the basic LSTM, stacked LSTM, BiLSTM, and stacked BiLSTM. Each model follows a neural network that consists of fully connected (FC) layers and a Softmax layer for feature fusion and spike/non-spike classification. The FC neural network is designed with a three-layer structure, the number of neurons are 500, 250, and 2, respectively. Fig. 7 shows the 4 LSTM network structures, respectively. We fully exploit the EEG signal and the SNE, MC features for spike detection by concatenating them in parallel as the input. The dimensions of EEG, SNE and MC are all 1×200, and the final feature sequence for model learning and spike detection is 3×200. The input feature dimension to the basic LSTM at each time step is 3×1.

For model learning and parameter optimization, the cross entropy is used as the loss function, and the adaptive moment estimation (ADAM) algorithm is used for parameter learning. ADAM combines the advantages of AdaGrad and RMSProp optimization algorithms, comprehensively considers the first and second-order moment estimation of the gradient, and updates the step size. The parameters are updated by

$$g_t = \nabla_\theta J(\theta_{t-1}) \tag{22}$$

$$m_t = \beta_1 \cdot m_{t-1} + (1 - \beta_1) \cdot g_t \tag{23}$$

$$v_t = \beta_2 \cdot v_{t-1} = (1 - \beta_2) \cdot g_t^2 \tag{24}$$

$$\hat{m}_t = \frac{m_t}{(1-\beta_1^t)},\ \hat{v}_t = \frac{v_t}{(1-\beta_2^t)} \tag{25}$$

$$\theta = \theta_{t-1} - \frac{\alpha \cdot \hat{m}_t}{\sqrt{\hat{v}_t} + \sigma} \tag{26}$$

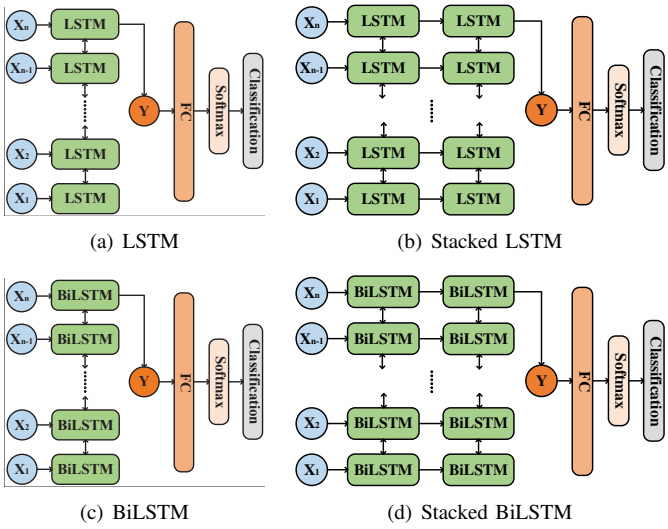

(a) LSTM (b) Stacked LSTM (c) BiLSTM (d) Stacked BiLSTM

Fig. 7. Four LSTM network based spike/non-spike classification models.

where g_t is the gradient of the current time step, θ_{t-1} is the parameter to be optimized obtained at the previous time step, m_t and v_t are the exponential moving average of the gradient and the gradient square, respectively, m_0 and v_0 are initialized to be 0, β_1 and β_2 are exponential decay rates, m_t and v_t are corrected to get $\hat{m}_t$ and $\hat{v}_t$, θ_t is the parameter updated at the current time step, α is the learning rate, σ is a positive value that tends to be 0 to avoid the division to be 0.

IV. Experiments and Discussions

A. Database

We test the spike detection performance on the EEGs of BECT patients recorded from the Children's Hospital, Zhejiang University School of Medicine (CHZU). There include the EEGs of 15 children (8 males and 7 females) suffered from the BECT syndrome, with the age ranging from 3 to 10 years old. The EEG acquisition equipment is Nicolet v32 with sampling frequency of 1000 Hz, and the electrodes are placed according to the international 10-20 system. The EEG data used in this experiment comes from the routine long-term EEG monitoring of inpatients in the hospital, and the duration is generally more than 10 hours. For each patient, a segment of EEGs around 10 minutes, that contain the most spikes, are used for testing. For instance, for patient 1, 163 spikes have been acquired in the 12 minutes 18 seconds EEG segment. All spikes are annotated by the help of neuroscientist from CHZU. Particularly, the detailed specifications of the CHZU BECT spike database are given in Table I.

To build the database, the patients EEG data is divided into three non-overlapping segments according to the amount of spikes in the time period, which are used to generate model training, verification and testing samples. The spike number ratio in each segment is 6:2:2. An equal amount of non-spike samples will be randomly generated in their respective data segments for training and verification. The time interval between the center point of the generated sample and the nearest peak point must be greater than 0.5 seconds. The non-spike samples will be generated with the same ratio to the

This article has been accepted for publication in a future issue of this journal, but has not been fully edited. Content may change prior to final publication. Citation information: DOI 10.1109/TNSRE.2021.3107142, IEEE Transactions on Neural Systems and Rehabilitation Engineering

TABLE I
SPECIFICATIONS OF THE CHZU BECT SPIKE DATABASE.

ID	Gender	Age	Duration	Spike discharge description	Number of spikes
1	M	9 y 3 m	12 m 18 s	Occasional discharge in T3, T5	163
2	F	9 y 1 m	13 m 51 s	Frequent discharges in C4, P4, T4, T6	1595
3	F	4 y 6 m	17 m 24 s	Occasionally discharges in C3, P3, T3, T5, C4	1174
4	M	7 y 3 m	21 m 43 s	Frequent discharges in C4, T4, T5	2033
5	M	6 y 6 m	34 m 12 s	Occasionally discharges in C3, P3, T3, T5	1709
6	M	10 y 6 m	10 m 6 s	Occasionally discharge in T3, T5	276
7	M	9 y 9 m	11 m 59 s	Frequent discharges in C3, P3, T3, T5	1696
8	F	9 y 7 m	14 m 27 s	Occasionally discharge in T3, T4	384
9	M	3 y 9 m	10 m 23 s	Frequent discharges in the C4, T4	610
10	M	8 y 5 m	8 m 45 s	Frequent discharges in C4, P4, T4, T6, T3	1478
11	M	6 y 5 m	15 m 51 s	Frequent discharges in T3	481
12	F	6 y 6 m	13 m 0 s	Occasionally discharges in C4, T4, T6	756
13	F	10 y 3 m	9 m 56 s	Frequent discharges in T3, T5, C3, P3, T4, T6	2334
14	F	8 y 10 m	17 m 11 s	Frequent discharges in T3, C3	1088
15	F	7 y 5 m	17 m 55 s	Frequent discharges in T3, T5, C4, P4, T4	1809

spikes in the training dataset. While for testing, the samples are directly derived from the real EEGs. The specific reasons have been explained in Section III.A.

B. Performance Evaluation

The sensitivity (Sens), precision (Prec) and F1 score are adopted for the performance evaluation, defined as

$$\text{Sens} = \frac{\text{TP}}{\text{TP}+\text{FN}},\ \text{Prec} = \frac{\text{TP}}{\text{TP}+\text{FP}},\ \text{F1} = \frac{2\text{Prec}\cdot\text{Sens}}{\text{Prec}+\text{Sens}}$$

where TP, FP, FN represent the true positive, false positive, and false negative, respectively.

It is noteworthy that unlike conventional spike detection algorithms that use manual labeling or candidate selection to obtain the testing sample for performance evaluation, the proposed method uses an overlapping continuous segmentation process to test performance. The advantage of the process is that it can more accurately reflect the detection performance of the algorithm, and at the meantime, can eliminate the dependence of the algorithm on the selection of candidate samples, which may involve a large number of complex threshold parameter adjustments. But it also suffers from the disadvantage that it is impossible to label all the generated samples one by one, and the automatic segmentation may result in incomplete waveforms. Therefore, under the premise of comprehensively considering the sample labeling, data segmentation, and actual detection application, we designed the following process to calculate the TP, TN, FP, and FN of the model through the pre-labeled spikes.

The first step is to divide samples containing spikes into two categories, correct and incorrect. Due to the way in sample segmentation, a spike frame may be contained in two adjacent samples. When the classification of at least one sample is a spike, their results are regarded as correct, otherwise the results are regarded as incorrect. In the second step, samples that do not contain spike are also divided into the above two categories. When these samples are classified as non-spike, the results are regarded as correct, otherwise the results are regarded as incorrect. The third step is to get the values of TP, TN, FP, and FN, where TP is the number of samples containing spikes in the database with correct results, and TN is the number of samples remaining in the database. FP is the number of samples with spikes in the database with incorrect results, and FN is the number of samples remaining in the database. For all experiments, the model is trained and tested on the patient-based, namely, for each patient, a model is learnt using his/her own data.

C. Experiment comparisons on feature input

The performance of the proposed algorithm on the feature inputs is firstly studied in this section. To show the contribution of the EEG signal and the two time domain features SNE and MC on spike detection, we test all the combinations of the three features, including the single feature by EEG, SNE, MC, the combinations of two features by EEG+SNE, EEG+MC, SNE+MC, as well as the combination of EEG+SNE+MC. The stacked BiLSTM neural network is adopted as the model for spike/non-spike classification. Table II lists the F1 score, sensitivity, and precision obtained by all these features of the 15 patients. The average spike detection results are also calculated for comparison. As observed, the top three performance rankings in all feature combinations are: EEG+SNE+MC, SNE+MC, and SNE. Among them, the model trained using EEG+SNE+MC achieves the best detection performance in general, where it obtains the highest F1 score and precision on 12 and 10 out of 15 patients, respectively, and the highest average F1 score and precision.

On one hand, the performance of time domain sequence features (SNE, MC) is better than using original EEG for spike detection, which proves the effectiveness and necessity of the two features extracted in the proposed algorithm. The model with SNE in the feature input performs better than the model with the same number of other features. On the other hand, generally speaking, more feature input will result in a model with better performance, which has been proved in combination performance rankings. However, the performance of the combination of EEG and SNE has declined compared with the model input by SNE alone. This is due to the different distributions of these two features. The mean value of EEG is zero and has values on the positive and negative semi-axes, but most of the SNE values are on the positive semi-axes. Due to the inability to unify the feature distribution, the neural network classifier cannot effectively use the information of the feature, thus, resulting in a degraded performance. At the same time, the weak representation ability of EEG is also a reason for the above problems. When replacing EEG with MC, the performance of the model has been significantly improved.

D. Experiment comparisons on LSTM architecture

The hyperparameters of the LSTM network usually affect the detection performance, include the number of hidden layer

This article has been accepted for publication in a future issue of this journal, but has not been fully edited. Content may change prior to final publication. Citation information: DOI 10.1109/TNSRE.2021.3107142, IEEE Transactions on Neural Systems and Rehabilitation Engineering

TABLE II
F1 SCORE, SENSITIVITY, PRECISION (%) WITH DIFFERENT FEATURES

	EEG	SNE	MC	EEG +SNE	EEG +MC	SNE +MC	EEG +SNE +MC
				Patient 1			
F1	68.12	89.11	86.96	81.08	78.83	89.31	**92.44**
Sens	92.16	97.83	**98.59**	83.33	94.74	97.26	96.49
Prec	54.02	81.82	77.78	78.95	67.50	82.56	**88.71**
				Patient 2			
F1	70.97	88.84	83.83	78.70	81.61	88.43	**92.52**
Sens	67.71	89.96	**97.81**	66.42	84.93	84.70	91.12
Prec	74.57	87.74	73.35	**96.54**	78.54	92.51	93.96
				Patient 3			
F1	62.46	77.63	63.23	75.34	65.50	75.77	**82.02**
Sens	57.74	79.91	78.00	77.02	64.61	79.65	**93.39**
Prec	68.02	**75.48**	53.17	73.72	66.41	72.26	73.12
				Patient 4			
F1	78.99	76.05	71.84	77.94	69.71	**89.46**	88.99
Sens	78.03	**98.11**	79.16	70.92	64.08	95.61	93.60
Prec	79.97	62.09	65.76	**86.51**	76.43	84.05	84.80
				Patient 5			
F1	71.69	76.05	71.55	84.75	64.01	84.90	**87.64**
Sens	82.48	**98.40**	83.86	85.32	56.46	86.58	85.39
Prec	63.40	61.98	62.40	84.19	73.90	83.28	**90.01**
				Patient 6			
F1	66.09	**89.75**	74.16	76.68	68.10	89.23	89.55
Sens	81.63	**99.41**	91.70	98.49	74.12	92.38	97.21
Prec	55.52	81.79	62.26	62.78	63.00	**86.30**	83.01
				Patient 7			
F1	78.38	89.27	79.71	90.46	84.42	90.06	**91.87**
Sens	89.16	96.47	**98.29**	94.61	94.98	95.54	90.22
Prec	69.93	83.07	67.04	86.65	75.97	85.17	**93.58**
				Patient 8			
F1	53.94	85.68	69.40	75.46	61.59	85.43	**86.60**
Sens	82.01	91.32	**98.82**	71.56	59.40	87.15	84.83
Prec	40.18	80.70	53.48	79.80	63.94	83.77	**88.44**
				Patient 9			
F1	80.46	88.67	81.25	92.56	81.48	86.71	**95.87**
Sens	91.79	**99.14**	99.40	97.21	81.13	99.44	98.08
Prec	71.62	80.20	68.70	88.33	81.83	76.87	**93.75**
				Patient 10			
F1	63.81	71.95	61.59	**82.27**	77.94	74.22	81.27
Sens	91.62	92.04	**95.45**	89.46	85.73	94.09	94.22
Prec	48.95	59.06	45.46	**76.15**	71.44	61.28	71.44
				Patient 11			
F1	64.29	77.76	63.71	77.49	69.06	80.90	**86.32**
Sens	85.71	**92.38**	91.04	87.32	80.30	88.67	85.42
Prec	51.43	67.13	49.00	69.65	60.57	74.38	**87.23**
				Patient 12			
F1	54.12	77.94	60.32	82.27	60.25	76.92	**85.27**
Sens	**92.32**	87.16	91.47	89.46	55.75	85.61	89.42
Prec	38.28	70.49	44.99	76.16	65.53	69.83	**81.49**
				Patient 13			
F1	66.39	87.94	76.46	86.84	85.84	87.37	**92.87**
Sens	86.28	**97.87**	95.57	94.93	89.35	97.83	97.53
Prec	53.95	79.84	63.71	80.01	82.60	78.94	**88.63**
				Patient 14			
F1	47.75	82.30	80.28	80.80	77.26	87.07	**89.58**
Sens	84.59	97.80	94.57	**98.32**	82.27	93.29	87.92
Prec	33.27	71.04	69.74	68.58	72.82	81.63	**91.30**
				Patient 15			
F1	51.61	80.24	70.49	81.15	62.11	81.95	**85.25**
Sens	86.29	**97.09**	93.29	95.60	82.79	94.76	95.83
Prec	36.81	68.38	56.64	70.50	49.69	72.20	**76.77**
				Average			
F1	65.27	82.61	72.99	81.59	72.51	84.51	**88.54**
Sens	83.30	**94.33**	93.47	86.67	76.71	91.50	92.04
Prec	55.99	74.05	60.90	78.57	70.01	79.00	**85.75**

units, activation function, learning rate, etc, where among them, the hidden layer units usually play the dominant role in the performance. With this regard, in this section, we test the spike detection performance of the aforementioned four LSTM neural network classification models with different size of memory units $\mu = [50 : 50 : 300]$. Fig. 8 shows the trend of F1 score of each model with respect to the memory unit size. All models can basically maintain stable performance when the memory unit size reaches 200, and continuously increasing the memory unit size will not significantly improve the performance. Compared with single-layer models, the stacked models can achieve better recognition performance, increasing F1 scores by 1.15% and 0.74% on the LSTM/BiLSTM network, respectively. But the advantage comes with the prices of more memory cell sizes and additional complexity. For BiLSTM and LSTM, the performance of the two networks using BiLSTM as the basis has a certain performance improvement compared with the network using LSTM under different memory units. The optimal performance on the single-layer model and the stacked model increased by 1.1% and 0.69%, respectively. The overall optimal spike detection model is the stacked BiLSTM with more than 200 memory cells.

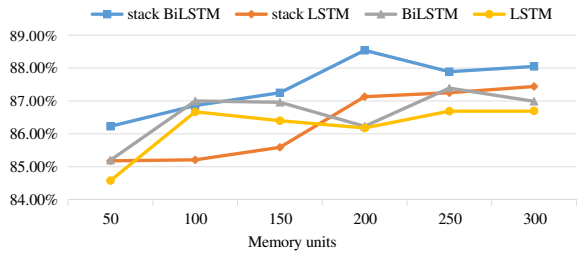

Fig. 8. The average F1 scores of spike detection with different memory units in the LSTM/BiLSTM models.

E. Experiment comparisons on SMOTE augmentation

In this section, the spike data augmentation method by SMOTE with different scale factors on the detection performance is studied. Particularly, the data enhancement ratio increases from 0 to 30 with an interval of 5. Fig. 9 shows the curves of F1 score, sensitivity, and precision. As observed, without spike data augmentation, the sensitivity of the model is high but the precision is low, which reflects the problem of high false alarm rate of the model. After adding the syntectic spikes on model training and validation, the F1 score and accuracy of the model have been significantly improved, but the sensitivity will first increase when the data scaling factor is small, and then decrease and maintain a relatively stable state when the scaling factor is higher than 15. Therefore, using data augmentation can significantly improve the spike detection performance and balance the false positive rate and the false negative rate. The SMOTE algorithm increases the amount of data to prevent the neural network model from overfitting and improves the generalization performance. At the same time, it adds random noise to the generated data in the time domain, which improves anti-interference ability of the model to a certain extent and makes the model more robust.

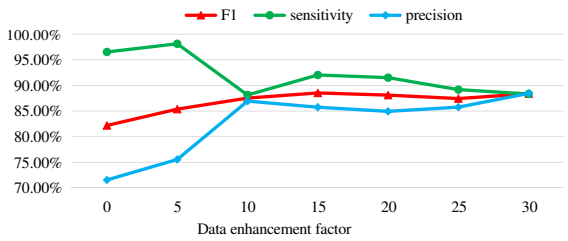

Fig. 9. The spike detection performance with respect to different spike data enhancement factors in SMOTE.

F. Experiment comparisons to SOTA methods

The last experiment shows the comparisons to 5 SOTA spike detection algorithms, including 1) spectral power feature

This article has been accepted for publication in a future issue of this journal, but has not been fully edited. Content may change prior to final publication. Citation information: DOI 10.1109/TNSRE.2021.3107142, IEEE Transactions on Neural Systems and Rehabilitation Engineering

method [32], 2) threshold methods based on the SNE [16] and MC features [13], respectively and 3) neural network classification method using FNN [37] and CNN [36], respectively.

The spectral power feature method [32] uses short-time Fourier transform (STFT) with 0.25 s time domain resolution and 4 Hz frequency domain resolution to extract the spectral power values of 8 frequency bands of the intracranial EEG, namely θ (4-8 Hz), α (8-13 Hz), β (13-30 Hz), γ_1 (30-56 Hz), γ_2 (64-116 Hz), rip1 (124 -176 Hz), rip2 (184-196 Hz), rip3 (204-236 Hz). STFT is used to obtain the sub-band spectral power of three time steps in the interval to be detected and its adjacent intervals, and merge them into a 3×8 feature matrix. The frequency domain features of 0.75 s EEG segment are obtained. Eventually, EEG segments will be divided into 4 categories (spike, RonS, ripple, baseline). Since the detection objective of the paper is on the relatively low-frequency spikes from the scalp EEGs, comparing with intracranial EEGs, there is a lot of interferences in the high-frequency part. Therefore, only the spectral powers of the first 5 frequency bands covering 4$\sim$116 Hz are extracted as features for performance testing in this section. The neural network classifier structure and hyperparameter settings are consistent with the BiLSTM in the proposed algorithm of the paper.

The threshold method is a traditional and widely used spike detection algorithm in the past. Without loss of generality, we used the SNE and MC as the features, and the threshold T_r used for detection is defined by the same way in [16] as

$$T_r = c\frac{1}{N}\sum_{n=1}^{N} F(n) \tag{27}$$

where N is the number of samples, c is a scaling factor selected by trials, and $F(n)$ is the feature sequence.

The neural network classification method uses two common structures, namely the fully connected neural network (FNN) and CNN. As FNN is generally not suitable for too high-dimensional data, we resized the three-dimensional features (3×200) to one-dimensional (1×600) as the input of FNN. The CNN structure is based on [36] but with certain improvements to better fit for the spike detection. First, the input features are passed through 3 convolution kernels with 1×40, 1×60, 1×80 kernel sizes, respectively, where the step size is $[1, 1]$. For further feature learning, the extracted features are then combined and input to 2 consecutive convolution kernels with the size of 3×3 and the steps of $[3, 1]$ and $[1, 1]$, respectively. Finally, a FNN is applied for spike/non-spike classification. The detailed network structures of FNN and CNN used in the paper are shown in Fig. 10.

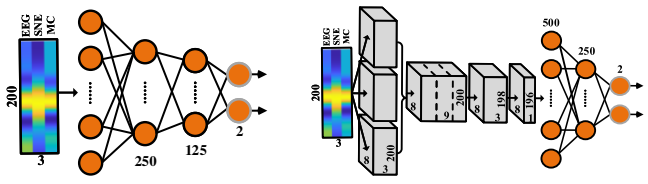

(a) FNN classification model (b) CNN classification model

Fig. 10. Structures of the FNN and CNN based spike detection algorithms.

TABLE III
F1 SCORE, SENSITIVITY, PRECISION (%) COMPARISONS TO THE SOTA SPIKE DETECTION ALGORITHMS.

	Proposed method	Spectral power feature method [32]	Threshold methods		Neural network classification methods	
			SNE [16]	MC [13]	FNN [37]	CNN [36]
	Patient 1					
F1	**92.44**	71.94	80.39	78.26	47.62	68.91
Sens	96.49	92.59	**98.80**	97.30	35.71	95.35
Prec	**88.71**	58.82	67.77	65.45	71.43	53.95
	Patient 2					
F1	**92.52**	88.18	88.36	79.16	69.80	84.51
Sens	91.12	92.42	**94.79**	85.53	55.59	84.01
Prec	**93.96**	84.32	82.74	73.67	93.79	85.01
	Patient 3					
F1	**82.02**	74.31	74.18	65.38	74.31	67.80
Sens	93.39	92.64	**96.05**	82.23	92.64	75.46
Prec	**73.12**	62.04	60.43	54.26	62.04	61.56
	Patient 4					
F1	88.99	**91.05**	80.10	75.79	57.64	83.90
Sens	**93.60**	86.25	91.56	83.50	57.92	85.27
Prec	84.80	**96.41**	71.19	69.38	57.36	82.58
	Patient 5					
F1	**87.64**	84.01	85.29	70.31	71.45	72.73
Sens	85.39	**96.11**	91.93	71.85	60.77	72.75
Prec	**90.01**	74.61	79.55	68.84	86.70	72.71
	Patient 6					
F1	89.55	89.80	**93.59**	83.94	68.40	85.33
Sens	97.21	**100.00**	93.39	80.42	68.64	92.54
Prec	83.01	81.50	**93.80**	87.79	68.15	79.16
	Patient 7					
F1	**91.87**	91.32	84.42	86.49	67.91	76.56
Sens	90.22	**90.82**	79.71	82.79	64.59	67.94
Prec	**93.58**	91.83	89.72	90.54	71.60	87.69
	Patient 8					
F1	**86.60**	82.36	81.51	83.46	59.36	68.57
Sens	84.83	89.70	77.13	75.24	54.80	**90.38**
Prec	88.44	76.13	86.41	**93.68**	64.76	55.23
	Patient 9					
F1	**95.87**	92.52	88.08	86.90	81.61	90.66
Sens	98.08	**98.97**	87.12	80.35	79.58	91.50
Prec	93.75	86.86	89.06	**94.61**	83.74	89.84
	Patient 10					
F1	**86.24**	**86.24**	71.32	75.19	65.24	68.82
Sens	**86.24**	**94.58**	86.20	65.06	65.48	84.68
Prec	**86.24**	79.26	60.82	**89.05**	65.00	57.97
	Patient 11					
F1	**86.32**	71.30	76.71	65.29	71.43	77.55
Sens	**85.42**	64.06	84.42	80.61	68.84	78.08
Prec	**87.23**	80.39	70.29	54.86	74.22	77.03
	Patient 12					
F1	**85.27**	79.14	81.19	59.92	59.66	70.52
Sens	89.42	85.56	86.02	**94.35**	55.78	67.39
Prec	**81.49**	73.61	76.86	43.90	64.12	73.94
	Patient 13					
F1	**92.87**	92.30	84.17	79.76	79.03	89.12
Sens	97.53	**97.54**	78.01	82.31	75.03	86.39
Prec	88.63	87.59	94.40	77.35	83.49	**92.03**
	Patient 14					
F1	**89.58**	87.21	85.38	77.82	62.84	77.90
Sens	87.92	**89.15**	83.08	84.15	74.12	69.11
Prec	**91.30**	85.35	87.81	72.37	54.54	89.26
	Patient 15					
F1	85.25	80.43	78.29	63.77	76.53	**85.41**
Sens	**95.83**	96.33	79.33	73.61	80.27	87.93
Prec	76.77	69.04	77.27	56.24	73.13	**83.03**
	Average					
F1	**88.54**	84.14	82.20	75.43	67.52	77.89
Sens	**92.04**	91.11	87.17	81.29	65.98	81.92
Prec	**85.75**	79.18	79.01	72.80	71.60	76.07

Table III shows the result comparisons to aforementioned SOTA spike detection algorithms. To have a fair comparison, the testing data division and the performance index calculations are the same to the previous experiments. As observed, the proposed algorithm can offer the highest F1 score on 11 out of 15 patients, the highest precision on 9 out of 15 patients. Meanwhile, for all patients, the proposed algorithm achieves the highest performance. Among all the 5 compared SOTA spike detection methods, the spectral power feature method has achieved good results on the database. Its average sensitivity is almost consistent with the proposed algorithm, but the average F1 score and precision are lower than the proposed algorithm. It is noted that the single sample duration of spectral power feature method (0.75 s) is longer than that

This article has been accepted for publication in a future issue of this journal, but has not been fully edited. Content may change prior to final publication. Citation information: DOI 10.1109/TNSRE.2021.3107142, IEEE Transactions on Neural Systems and Rehabilitation Engineering

of the proposed algorithm (0.2 s), meaning that the proposed algorithm can locate spikes more accurately with a better resolution. The frequency domain features used in this method are obtained through STFT. To improve the positioning ability of the algorithm, the time domain resolution of the STFT needs to be increased, which will result in a decrease in frequency resolution. Therefore, the spectral power of each frequency band cannot be accurately extracted, which may lead to the loss of accuracy. Generally speaking, unless using high sampling frequency EEG, it is impossible to further improve the spike location ability of the proposed algorithm. The two threshold methods have achieved promising results on some patient data with obvious spike. However, there are low-amplitude spikes in real data. The waveform is similar to a typical spike but the peak amplitude is slightly higher than normal EEGs. The existence of a large number of such spikes makes the selection of the threshold very difficult, resulting in performance degradation. While for the two mainstream neural network classifiers, neither FNN nor CNN can achieve satisfactory results. Unlike LSTM, these two neural networks are unable to make good use of the time series information contained in the EEG signals. In the other words, LSTM is more effective in time series data learning. From the results, it is also observed that all methods suffered performance fluctuations among different patients. The reason behind is the existence of the aforementioned low-amplitude spikes. The features used in the proposed algorithm as well as in the compared SOTA methods are insufficient in characterizing such spikes.

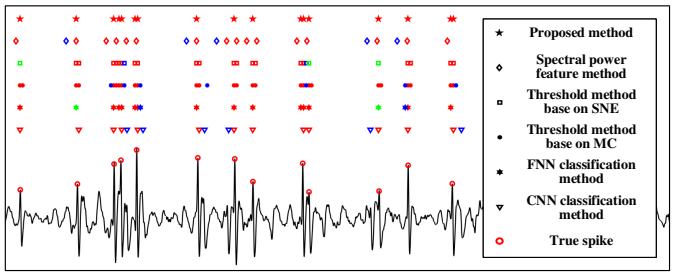

Fig. 11. Screenshot on the real-time spike detection performance on the CHZU database, where the green color represents false negatives, the blue color represents false positives, and the red color indicates the true positive.

Particularly, Fig. 11 shows a screenshot on the real-time detection performance obtained from the CHZU database, where comparisons between the proposed algorithm and the 5 SOTA methods are presented. The testing EEG segment includes 13 true spike discharges, and different colors are used to annotate the detection results, where the green, blue and red colors represent the false negatives, the false positives, and the true positive, respectively. As depicted, the proposed method successfully detects the all the EEG frames containing the 16 true spike discharges without false alarms. The compared frequency domain feature method, the threshold method using the MC EEG feature, and the CNN classification method have high sensitivity, but also suffer some false alarms in the EEG frames adjacent to the spike discharge frames. For the threshold method using the SNE EEG feature and the FNN classification method, both of them have problems of high false positive and false negative rates. It is also observed that the spike detection resolution of the frequency domain feature method is lower than other methods, making it not suitable for accurate spike localization.

V. Conclusions

This paper proposed a novel BECT spike detection algorithm composed of time domain EEG sequence features extraction and neural network classifier based on LSTM architecture. Aiming at the problem of data imbalance in spike detection, the SMOTE algorithm has been applied in the proposed algorithm for the spike sample augmentation. Based on the characteristics of the scalp EEG and spikes, two time-domain EEG sequence features that are effective in characterizing spikes have extracted. These features are fused for spike representation and a stacked BiLSTM has been developed for spike/non-spike classification. The effectiveness of the proposed algorithm has been verified on the EEG database of 15 BECT patients recorded from the CHZU. The comparison experiments shown that the algorithm has higher detection sensitivity, precision and F1 score, and has stronger robustness than many SOTA spike detection methods. In the future, more attentions will be paid to enhancing the algorithm's anti-interference ability and recognition ability on low-amplitude spikes. Meanwhile, more effective algorithms on addressing the spike data imbalance and exploring the impact of data augmentation on the overall recognition ability will be studied.

Ethical Standards

This study has been approved by the Second Affiliated Hospital of Zhejiang University and registered in Chinese Clinical Trail Registry (ChiCTR1900020726). All patients gave their informed consent prior to their inclusion in the study.

References

[1] P. Santanelli, M. Bureau, A. Magaudda, G. Gobbi, and J. Roger, "Benign partial epilepsy with centrotemporal (or rolandic) spikes and brain lesion," *Epilepsia*, vol. 30, no. 2, pp. 182–188, 1989.

[2] S. Völkl-Kernstock, S. Bauch-Prater, E. Ponocny-Seliger, and M. Feucht, "Speech and school performance in children with benign partial epilepsy with centro-temporal spikes (bcects)," *Seizure*, vol. 18, no. 5, pp. 320–326, 2009.

[3] J. S. Ebersole and T. A. Pedley, *Current practice of clinical electroencephalography*. Lippincott Williams & Wilkins, 2003.

[4] J. Hao, Y. Cui, B. Niu, L. Yu, Y. Lin, Y. Xia, D. Yao, and D. Guo, "Roles of very fast ripple (500-1000hz) in the hippocampal network during status epilepticus," *International Journal of Neural Systems*, vol. 31, no. 04, p. 2150002, 2021.

[5] T. C. Technologies, "10/20 system positioning manual." 2012.

[6] L. C. Fonseca, G. M. A. Tedrus, E. M. d. C. Pacheco, M. F. Berretta, A. A. Campregher, and D. M. Costa, "Benign childhood epilepsy with centro-temporal spikes: correlation between clinical, cognitive and eeg aspects," *Arquivos de Neuro-psiquiatria*, vol. 65, no. 3A, pp. 569–575, 2007.

[7] Y. Lin, P. Du, H. Sun, Y. Liang, Z. Wang, Y. Cui, K. Chen, Y. Xia, D. Yao, L. Yu, and D. Guo, "Identifying refractory epilepsy without structural abnormalities by fusing the common spatial patterns of functional and effective eeg networks," *IEEE Transactions on Neural Systems and Rehabilitation Engineering*, vol. 29, pp. 708–717, 2021.

[8] D. Samanta and Y. Al Khalili, "Electrical status epilepticus in sleep (eses)," *StatPearls [Internet]*, 2019.

[9] S. Li, W. Zhou, Q. Yuan, and Y. Liu, "Seizure prediction using spike rate of intracranial eeg," *IEEE Transactions on Neural Systems and Rehabilitation Engineering*, vol. 21, no. 6, pp. 880–886, 2013.

This article has been accepted for publication in a future issue of this journal, but has not been fully edited. Content may change prior to final publication. Citation information: DOI 10.1109/TNSRE.2021.3107142, IEEE Transactions on Neural Systems and Rehabilitation Engineering

[10] J. R. Stevens, B. L. Lonsbury, and S. L. Goel, "Seizure occurrence and interspike interval: telemetered electroencephalogram studies," *Archives of neurology*, vol. 26, no. 5, pp. 409–419, 1972.

[11] J. Gotman and L.-Y. Wang, "State dependent spike detection: validation," *Electroencephalography and clinical neurophysiology*, vol. 83, no. 1, pp. 12–18, 1992.

[12] J. Qian, J. S. Barlow, and M. P. Beddoes, "A simplified arithmetic detector for eeg sharp transients-preliminary results," *IEEE transactions on biomedical engineering*, vol. 35, no. 1, pp. 11–18, 1988.

[13] X. Liu, X. Yang, and N. Zheng, "Automatic extracellular spike detection with piecewise optimal morphological filter," *Neurocomputing*, vol. 79, pp. 132–139, 2012.

[14] V. P. Oikonomou, A. T. Tzallas, and D. I. Fotiadis, "A kalman filter based methodology for eeg spike enhancement," *Computer methods and programs in biomedicine*, vol. 85, no. 2, pp. 101–108, 2007.

[15] A. K. Keshri, R. K. Sinha, A. Singh, and B. N. Das, "Dfaspike: A new computational proposition for efficient recognition of epileptic spike in eeg," *Computers in biology and medicine*, vol. 41, no. 7, pp. 559–564, 2011.

[16] H. Azami and S. Sanei, "Spike detection approaches for noisy neuronal data: assessment and comparison," *Neurocomputing*, vol. 133, pp. 491–506, 2014.

[17] M. I. Khalid, T. Alotaiby, S. A. Aldosari, S. A. Alshebeili, M. H. Al-Hameed, F. S. Y. Almohammed, and T. S. Alotaibi, "Epileptic meg spikes detection using common spatial patterns and linear discriminant analysis," *IEEE Access*, vol. 4, pp. 4629–4634, 2016.

[18] A. Chahid, F. Albalawi, T. N. Alotaiby, M. H. Al-Hameed, S. Alshebeili, and T.-M. Laleg-Kirati, "Qupwm: Feature extraction method for epileptic spike classification," *IEEE journal of biomedical and health informatics*, vol. 24, no. 10, pp. 2814–2824, 2020.

[19] A. Nonclercq, M. Foulon, D. Verheulpen, C. De Cock, M. Buzatu, P. Mathys, and P. Van Bogaert, "Cluster-based spike detection algorithm adapts to interpatient and intrapatient variation in spike morphology," *Journal of neuroscience methods*, vol. 210, no. 2, pp. 259–265, 2012.

[20] M. Soleimani, A. Vahidi, and B. Vaseghi, "Two-dimensional stockwell transform and deep convolutional neural network for multi-class diagnosis of pathological brain," *IEEE Transactions on Neural Systems and Rehabilitation Engineering*, vol. PP, pp. 1–1, 11 2020.

[21] D. Wang, Z. Liu, Y. Tao, W. Chen, B. Chen, Q. Wang, X. Yan, and G. Wang, "Improvement in eeg source imaging accuracy by means of wavelet packet transform and subspace component selection," *IEEE Transactions on Neural Systems and Rehabilitation Engineering*, vol. 29, pp. 650–661, 2021.

[22] L. Logesparan and E. RodriguezVillegas, "A novel phase congruency based algorithm for online data reduction in ambulatory eeg systems," *IEEE Transactions on Biomedical Engineering*, vol. 58, no. 10, pp. 2825–2834, 2011.

[23] K. Kobayashi, J. Jacobs, and J. Gotman, "Detection of changes of high-frequency activity by statistical time-frequency analysis in epileptic spikes," *Clinical Neurophysiology*, vol. 120, no. 6, pp. 1070–1077, 2009.

[24] C. D. Richard, A. Tanenbaum, B. Audit, A. Arneodo, A. Khalil, and W. N. Frankel, "Swdreader: A wavelet-based algorithm using spectral phase to characterize spike-wave morphological variation in genetic models of absence epilepsy," *Journal of Neuroscience Methods*, vol. 242, pp. 127–140, 2015.

[25] Y. Yuan, C. Yang, and J. Si, "The m-sorter: An automatic and robust spike detection and classification system," *Journal of Neuroscience Methods*, vol. 210, no. 2, pp. 281–290, 2012.

[26] J. Cao, D. Hu, Y. Wang, J. Wang, and B. Lei, "Epileptic classification with deep transfer learning based feature fusion algorithm," *IEEE Transactions on Cognitive and Developmental Systems*, pp. 1–1, 2021.

[27] J. Cao, J. Zhu, W. Hu, and A. Kummert, "Epileptic signal classification with deep EEG features by stacked CNNs," *IEEE Transactions on Cognitive and Developmental Systems*, vol. 12, no. 4, pp. 709–722, 2020.

[28] D. Hu, J. Cao, X. Lai, Y. Wang, S. Wang, and Y. Ding, "Epileptic state classification by fusing hand-crafted and deep learning EEG features," *IEEE Transactions on Circuits and Systems II: Express Briefs*, pp. 1–1, 2020.

[29] D. Hu, J. Cao, X. Lai, J. Liu, S. Wang, and Y. Ding, "Epileptic signal classification based on synthetic minority oversampling and blending algorithm," *IEEE Transactions on Cognitive and Developmental Systems*, pp. 1–1, 2020.

[30] W. Webber, B. Litt, K. Wilson, and R. P. Lesser, "Practical detection of epileptiform discharges (eds) in the eeg using an artificial neural network: a comparison of raw and parameterized eeg data," *Electroencephalography and clinical Neurophysiology*, vol. 91, no. 3, pp. 194–204, 1994.

[31] Ö. Özdamar and T. Kalayci, "Detection of spikes with artificial neural networks using raw eeg," *Computers and Biomedical Research*, vol. 31, no. 2, pp. 122–142, 1998.

[32] A. Medvedev, G. Agoureeva, and A. Murro, "A long short-term memory neural network for the detection of epileptiform spikes and high frequency oscillations," *Scientific reports*, vol. 9, no. 1, pp. 1–10, 2019.

[33] W. Gao, T. Yu, J.-G. Yu, Z. Gu, K. Li, Y. Huang, Z. L. Yu, and Y. Li, "Learning invariant patterns based on a convolutional neural network and big electroencephalography data for subject-independent p300 brain-computer interfaces," *IEEE Transactions on Neural Systems and Rehabilitation Engineering*, 2021.

[34] J. R. Paulo, G. Pires, and U. J. Nunes, "Cross-subject zero calibration drivers drowsiness detection: Exploring spatiotemporal image encoding of eeg signals for convolutional neural network classification," *IEEE transactions on neural systems and rehabilitation engineering*, 2021.

[35] L. Yang, Y. Song, K. Ma, and L. Xie, "Motor imagery eeg decoding method based on a discriminative feature learning strategy," *IEEE Transactions on Neural Systems and Rehabilitation Engineering*, vol. 29, pp. 368–379, 2021.

[36] A. R. Johansen, J. Jin, T. Maszczyk, J. Dauwels, S. S. Cash, and M. B. Westover, "Epileptiform spike detection via convolutional neural networks," in *2016 IEEE International Conference on Acoustics, Speech and Signal Processing (ICASSP)*. IEEE, 2016, pp. 754–758.

[37] M. Saif-ur Rehman, R. Lienkämper, Y. Parpaley, J. Wellmer, C. Liu, B. Lee, S. Kellis, R. Andersen, I. Iossifidis, T. Glasmachers *et al.*, "Spikedeeptector: a deep-learning based method for detection of neural spiking activity," *Journal of neural engineering*, vol. 16, no. 5, p. 056003, 2019.

[38] M. Rácz, C. Liber, E. Németh, R. Fiáth, J. Rokai, I. Harmati, I. Ulbert, and G. Márton, "Spike detection and sorting with deep learning," *Journal of neural engineering*, vol. 17, no. 1, p. 016038, 2020.

[39] Z. Wang, D. Wu, F. Dong, J. Cao, T. Jiang, and J. Liu, "A novel spike detection algorithm based on multi-channel of BECT EEG signals," *IEEE Transactions on Circuits and Systems II: Express Briefs*, vol. 67, no. 12, pp. 3592–3596, 2020.

[40] J. Cao, L. Chen, D. Hu, F. Dong, T. Jiang, W. Gao, and F. Gao, "Unsupervised eye blink artifact detection from eeg with gaussian mixture model," *IEEE Journal of Biomedical and Health Informatics*, vol. 25, no. 8, pp. 2895–2905, 2021.

[41] J. Wang, J. Cao, D. Hu, T. Jiang, and F. Gao, "Eye blink artifact detection with novel optimized multi-dimensional electroencephalogram features," *IEEE Transactions on Neural Systems and Rehabilitation Engineering*, vol. 29, pp. 1494–1503, 2021.

[42] N. V. Chawla, K. W. Bowyer, L. O. Hall, and W. P. Kegelmeyer, "S-mote: synthetic minority over-sampling technique," *Journal of artificial intelligence research*, vol. 16, pp. 321–357, 2002.

[43] J. F. Kaiser, "On a simple algorithm to calculate the'energy'of a signal," in *International conference on acoustics, speech, and signal processing*. IEEE, 1990, pp. 381–384.

[44] S. Mukhopadhyay and G. Ray, "A new interpretation of nonlinear energy operator and its efficacy in spike detection," *IEEE Transactions on biomedical engineering*, vol. 45, no. 2, pp. 180–187, 1998.

[45] J. Serra, "Introduction to mathematical morphology," *Computer vision, graphics, and image processing*, vol. 35, no. 3, pp. 283–305, 1986.

[46] S. Hochreiter, "The vanishing gradient problem during learning recurrent neural nets and problem solutions," *International Journal of Uncertainty, Fuzziness and Knowledge-Based Systems*, vol. 6, no. 02, pp. 107–116, 1998.